Nanoscale

PAPER

View Article Online
View Journal | View Issue

Check for updates

Cite this: *Nanoscale*, 2021, **13**, 5344

Impact of dynamic sub-populations within grafted chains on the protein binding and colloidal stability of PEGylated nanoparticles†

Delyan R. Hristov,‡[a] Hender Lopez,[b] Yannick Ortin,[c] Kate O'Sullivan,[c] Kenneth A. Dawson*[a] and Dermot F. Brougham*[c]

Received 20th November 2020,
Accepted 24th January 2021

DOI: 10.1039/d0nr08294e

rsc.li/nanoscale

Polyethylene glycol grafting has played a central role in preparing the surfaces of nano-probes for biological interaction, to extend blood circulation times and to modulate protein recognition and cellular uptake. However, the role of PEG graft dynamics and conformation in determining surface recognition processes is poorly understood primarily due to the absence of a microscopic picture of the surface presentation of the polymer. Here a detailed NMR analysis reveals three types of dynamic ethylene glycol units on PEG-grafted SiO_2 nanoparticles (NPs) of the type commonly evaluated as long-circulating theranostic nano-probes; a narrow fraction with fast dynamics associated with the chain ends; a broadened fraction spectrally overlapped with the former arising from those parts of the chain experiencing some dynamic restriction; and a fraction too broad to be observed in the spectrum arising from units closer to the surface/graft which undergo slow motion on the NMR timescale. We demonstrate that ethylene glycol units transition between fractions as a function of temperature, core size, PEG chain length and surface coverage and demonstrate how this distribution affects colloidal stability and protein uptake. The implications of the findings for biological application of grafted nanoparticles are discussed in the context of accepted models for surface ligand conformation.

Published on 22 February 2021. Downloaded by TU Dublin on 4/4/2022 10:07:53 AM.

Introduction

The widespread application of hydrophilic polymer surface coatings, such as polyethylene glycol (PEG), on medical device surfaces, bionanostructures, and biomolecular medicines has been viewed primarily as a practical means to mitigate a broad range of undesirable biological responses to foreign bodies.[1–11] PEG is believed to present a stable hydrogen-bonded hydration layer which, combined with the configurational entropy derived from the flexible chains, inhibits protein adsorption, as well as screening antigenic epitopes (that might be caught up in the interface layer) from immunological processing.[5,12] Beneficial effects, such as the prolongation of bloodstream circulation and reduced probability of implant rejection, were conceived to derive from a reduction in the degree of non-specific biomolecular binding and few attempts were made to uncover the detailed mechanisms involved beyond that.[7,13–18]

Several significant changes in thinking have emerged recently. Firstly scientific developments now suggest that biological recognition of nanoscale surfaces entails levels of complexity and subtlety not previously recognised. For example, the identity of the protein corona may influence drug release profiles.[19] Blood circulation times may require the recognition of specific proteins or protein motifs on the particle surface.[20] Conversely other proteins may lead to a lower probability of recognition and longer nanoparticle (NP) circulation times *in vivo*.[5] The complexity is well described in the work of Cai *et al.*, where the authors suggest that "appropriate surface ligands with reduced protein binding and desired long blood circulation time could be predicted from acquired corona composition".[21]

The growing set of methodologies available to study these phenomena at the molecular level has enabled deeper understanding of surface effects.[5,19,20,22–25] For example, new NMR tools have enabled more detailed analysis of the particle surface and its interactions with low affinity proteins.[3,26–28] There have also been several observations, discussed below,

[a]*Centre for BioNano Interactions, School of Chemistry, University College Dublin, Dublin, Republic of Ireland*
[b]*School of Physics & Optometric & Clinical Sciences, Technological University Dublin, City Campus, Kevin Street, Dublin 8, Republic of Ireland*
[c]*School of Chemistry, University College Dublin, Belfield, Dublin 4, Republic of Ireland. E-mail: dermot.brougham@ucd.ie*
†Electronic supplementary information (ESI) available. See DOI: 10.1039/d0nr08294e
‡Present address: Department of Engineering, University of Massachusetts, Boston, United States of America.

This journal is © The Royal Society of Chemistry 2021

Published on 22 February 2021. Downloaded by TU Dublin on 4/4/2022 10:07:53 AM.

that cast a new light on previous understanding.[3–5,29–32] In particular, questions about how interactions with environmental molecules are influenced by the ligand coverage (surface density) and conformation have been raised.

The original paradigm of nanoscale biomolecular recognition that was framed around the 'biomolecular corona'[24] may be briefly summarised as follows. Those environmentally derived biomolecules presented 'accessibly'[22,23] on the nanoparticle surface with residence times exceeding a critical 'processing time' are deemed to be involved in biological recognition and processing and termed 'hard corona', whereas those that exchange faster are termed 'soft corona' and while they affect physicochemical aspects of the material they are unlikely to contribute directly to recognition. This conception while in broad terms being verified across many fields, has mainly been considered for conventional strongly adsorbing nanostructures[33] where the separation of timescales between the strongly adsorbed hard corona and loosely associated soft corona is great. In the present case of PEG layers, the application of these fundamental ideas is more nuanced. For instance, while it is evident that the 'steady state amount' of exchanging biomolecules in the polymeric layer could affect gross issues, such as circulation time, the modern focus derives from the certain realisation that PEG layers *in situ* are biologically recognised, and the strong suspicion that the very small amounts of biomolecule implicated in the layer are critical to that mechanism.[3,5] Thus a major interest now is in understanding how (in the above context) those small amounts of biomolecules are presented in the low binding layer and the underlying layer where exchange times are moderate.[26] It is clear that these issues cannot be fully clarified without a detailed molecular understanding of the structure and dynamics of tethered low binding affinity surfaces, such as PEG ligand layers.

PEG layers on flat surfaces have been extensively studied using techniques such as QCM,[34] surface force apparatus[35–37] and atomic force microscopy,[38] revealing that PEG coverage largely determines surface properties such as surface friction and protein binding.[12,39] It is suggested that these responses are primarily determined by ligand conformation and solvent-layer interactions.[12,40] While those methods are not feasible for studying particle dispersions, other evidence, including protein binding and cell response studies, points to significant influence of ligands on nanoparticle responses.[3,41–43]

In particular ^{1}H NMR has previously been used,[42,44–46] in conjunction with other methods,[47] to study ligand grafts on dispersed nanoparticles. However, the majority of studies are for small particles (<20 nm) and small molecules (<1000 Da). In these cases, the observed NMR signal broadening arises from: (i) the presence of multiple environments (usually due to different adsorption sites)[48–51] and (ii) magnetic susceptibility effects, both of which generate heterogeneous broadening. In addition there can be effects due to: (iii) ligand exchange; (iv) residual dipolar interactions; and (v) particle–ligand electronic interactions, usually resulting in homogeneous broadening.[48,52] In cases where these interactions dominate the resonances are not detectable by conventional high resolution NMR, and specialized magic angle spinning techniques are required.[44] ^{1}H MAS NMR spectroscopy[53] has been used for qualitative identification of species present on 5 nm Fe_3O_4 nanoparticles.[44] ^{31}P CP-MAS NMR was used to identify multiple surface binding sites for 1.8 nm triphenylphosphine stabilized Au nanoparticles,[54] which were shown by hole-burning to be primarily heterogeneously broadened due to a distribution of chemical environments. ^{19}F NMR spectroscopy of particle bound ligands has recently been used to measure the effect of protein adsorption on diffusion.[26]

Conventional high-resolution solution state NMR is a more commonly available technique suitable for ligand analysis and potentially quantitation. ^{1}H and ^{13}C NMR has recently been used, in combination with other techniques,[55] to study the mobility and conformation of ligands[48,50] and to evaluate surface composition for mixed ligand systems.[49,56] For instance, in the study of patchy 4–5 nm Au particles the Stellacci Group used the dependence of the chemical shift and nuclear Overhauser effect enhancements on ligand mole fraction to confirm patch formation and/or ligand dispersion for combinations of ligands exhibiting different phase compatibility.[49] Salorinne and co-workers identified all 44 possible ^{1}H resonances arising from Au_{102} nanoparticles surface grafted with *para*-mercaptobenzoic acid.[50] These high-resolution NMR studies, which were at the edge of the spectral resolution achievable for these particle sizes, establish the suitability of the technique to measure ligand dynamics and conformations. There are some NMR studies of lipid nanoparticles,[57,58] however there are surprisingly few studies into PEG dynamics for higher molecular weight grafts and for larger particles, which is the size range of greatest interest for bio-probe development and in which broadening begins to dominate.

Here we describe the synthesis and grafting of silica particles with varied surface coverage of higher molecular weight PEG, and provide detailed ^{1}H NMR analysis of the grafts. Spectra were recorded at different temperatures for PEG (M_w 1 and 5 kDa) bound to relatively large (50, 65, 75, 90 and 200 nm core diameter) nanoparticles with varied surface coverage (0.05 to 1.0 PEG chains per nm^2). Particular care was taken to evaluate the sensitivity of the outcomes to the model selected for fitting the spectra and to confirm the interpretation of changes in chain segment mobility by T_1 and T_2 relaxometry. We demonstrate that ethylene glycol units can be separated into three distinct quantifiable dynamic fractions whose relative populations change with coverage and temperature in a predictable way, providing insight into the molecular changes associated with changes in brush conformation. Finally we show that for 50 nm SiO_2 PEG_{5000} nanoparticles there was measurable coverage dependence in (serum) protein uptake and distribution. These findings suggest that coverage-induced changes in PEG dynamics, and particularly in the population of the dynamic fractions, alter the critical residence times and hence recognition for different proteins in subtly different ways. The implications of the findings for function of grafted nanoparticles in biological systems are discussed.

Published on 22 February 2021. Downloaded by TU Dublin on 4/4/2022 10:07:53 AM.

Results

Sample preparation and colloidal characterization

Silica cores were synthesized as previously described.[41,59] PEG molecules were attached through the addition of a silane-functionalized PEG, as previously described.[41] PEGylated particles were washed using five centrifugation re-suspension cycles (which is in excess of the number usually applied) to carefully remove contaminants, including precursors.[29] The removal of free PEG and the loss of some particles during this process were evaluated by NMR; we observed that in all cases more than 94% of the total NMR signal was lost after the third wash (Fig. S1†). Typically the intensity of the free PEG signal in the last supernatant was between 1–4% of that measured for the subsequently redispersed pellet (Fig. S2†). Finally, comparison of the line-shape analysis from the particle suspension and last supernatant shows that a maximum of 3% of the integral value in the last supernatant has the chemical shift and linewidth of free PEG (Fig. S3†). This suggests that free PEG contributes <0.12% to the PEG signal of the particle suspensions immediately after synthesis and purification.

The final particle suspensions were observed to be fully dispersed in water with narrow size distributions, by dynamic light scattering (DLS), and to be colloidally stable for several weeks (Table 1, S1, Fig. S4 and S5†). Nanoparticle suspensions with different coverage were synthesized using the same batch of core particles to which different concentrations of PEG were added. The average coverage was determined by quantitative ^{1}H NMR of dissolutes using the previously described procedure.[29] The coverage was found to vary from 0.06 to 0.35 nm^{-2} (for PEG_{5000} on 50 nm NPs), which corresponds in all cases to the "brush" conformation under the accepted criteria.[60–62] Unless otherwise indicated we describe the response of suspensions of 50 nm cores, which is in the size range of interest for drug delivery and diagnostics, grafted with PEG_{5000}.

^{1}H NMR lineshape analysis

The effect of coverage and chain length on the ^{1}H spectra was evaluated; variation in PEG coverage and color coding is schematically represented in Fig. 1a. For all D_2O suspensions it is immediately apparent (Fig. 1) that binding to the particle surface results in changes to the ethylene group resonance at *c.* 3.7 ppm,[7,29] as compared to free PEG solutions (Fig. S6†). Visual inspection indicates that for most suspensions, *e.g.* Fig. 1b, the resonance has two distinct Lorentzian-like contributions from narrow and broad fractions. This suggests different dynamic environments for PEG associated either with different populations on a given particle or different types of particles. Care was taken therefore to use extended recycle

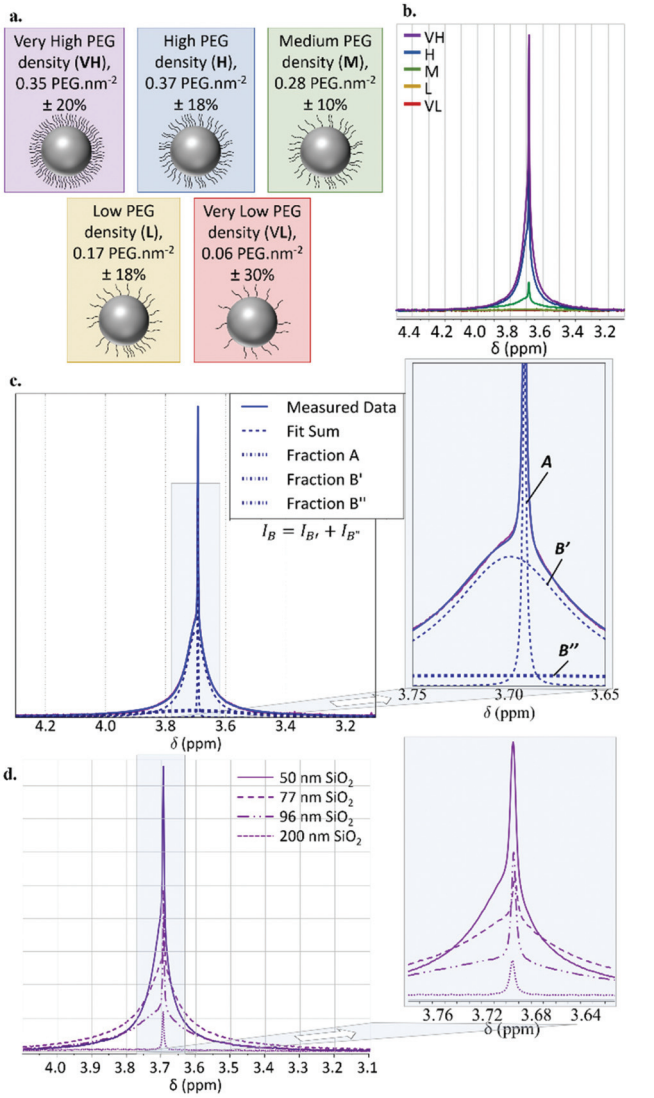

Fig. 1 Regions of interest in the ^{1}H spectra, recorded at 25 °C for PEG_{5000} grafted SiO_2 nanoparticles in D_2O suspension. (a) Schematic representation of 50 nm PEG_{5000} grafted SiO_2 nanoparticles showing the colour coding used in the rest of this work; VH (purple), H (blue), M (green), L (dark yellow) and VL (dark red). (b) Representative spectra recorded at 25 °C for 50 nm particles of different coverage. (c) A representative line fit for a VH spectrum for 50 nm particles showing the measured signal (purple), the sum of the fractions (blue dashes), and the individual fractions (navy dots and dashes). (d) Change in the spectra with PEG_{5000}/particle size ratio, the insert highlights the change in broadness of fraction *B* with particle size.

Table 1 Physicochemical characterisation (DLS) and PEG coverage, for N = 8 NP batches

	Size characterisation, DLS			
Sample	*Z* average diameter (nm)	PDI	Number mean diameter (nm)	ρ_{PEG} (nm^{-2})
VH	92 ± 12	0.09 ± 0.05	70 ± 8	0.35 ± 0.07
H	101 ± 23	0.11 ± 0.07	68 ± 9	0.37 ± 0.06
M	97 ± 15	0.10 ± 0.06	74 ± 20	0.28 ± 0.02
L	111 ± 22	0.16 ± 0.08	73 ± 19	0.17 ± 0.04
VL	113 ± 39	0.20 ± 0.08	57 ± 3	0.06 ± 0.02
SiO_2 core	95 ± 21	0.16 ± 0.08	61 ± 12	0

This journal is © The Royal Society of Chemistry 2021

Published on 22 February 2021. Downloaded by TU Dublin on 4/4/2022 10:07:53 AM.

delays, of 25 s, in the experiments to enable quantitation in case of spectral contributions with long T_1 values.

Multi-Lorentzian fitting successfully reproduced the lineshape confirming that for all but the lowest coverages the signal comprises a narrow fraction (*A*, FWHM ≤4 Hz unshifted relative to free PEG) and a broad fraction (*B*, FWHM ≥30 Hz, shifted downfield by *c.* 0.01 ppm). Fraction *A* is almost perfectly fitted by a single Lorentzian while fraction *B* is best fit by two Lorentzians (Fig. 1c). Increasing the number of functions used in the fitting does not measurably change the quantification of *A* and *B* that follows (see Fig. S7† for details).

We found that for fixed core size and PEG chain length an increase of coverage leads to: (i) fraction *A* becoming more prominent (Fig. S8g†) compared to *B*; (ii) the broadness decreasing slightly (Fig. S8i†); and (iii) the mean chemical shift (δ) value shifting upfield (Fig. S8h†). Similar trends were clearly observed (despite reduced signal-to-noise) for PEG_{1000} grafted 50 nm NPs (Fig. S8d, e, f, S9 and S10†), demonstrating the presence of similar coverage dependence for narrow and broad fractions for shorter grafts. One difference for PEG_{1000} as compared to PEG_{5000} grafts is that the signal broadened with reducing ligand coverage. Increasing the particle size (for PEG_{5000}) resulted in broadening of fraction *B* (Fig. 1d and S8–10†).

Comparison of the total ^{1}H signal intensity of the NP suspensions and their dissolute solutions demonstrates the presence of a third fraction, *C*, not detectable in the suspensions which is apparently broadened into the baseline. This presence of *C* can be confirmed, and its spectral profile estimated, through point-by-point ^{1}H saturation transfer experiments. Typical PEG and HDO saturation profiles (integral as a function of the selective saturation pulse frequency) for a **VH** suspension are shown in Fig. S11.†

Interestingly, for **VH**, **H** and **M** suspensions the methoxy end group is observable (for ν_L 600 MHz) as a very weak sharp feature at *c.* 3.3 ppm. For **L** this feature is rarely detectable at room temperature, but often becomes observable at higher temperature, (Fig. S12†). The observations for the ethylene and methoxy resonances suggest complex evolution of chain-surface interactions, leading to freer motions for a greater faction of the graft-distant units at higher coverage and temperature. At the lowest coverage the NMR response is qualitatively different.

The ^{1}H spectra are consistent with the presence of three fractions arising due to differences in PEG mobility or surface conformation. We suggest that fraction *A* is the most mobile and arises from ethylene glycol units furthest away from the particle surface, fraction *B* arises from units closer in and fraction *C* from the most conformationally restrained units nearest the particle surface.

Temperature dependence of the 1H spectra

To better understand the nature of the fractions and to further probe the sensitivity of the spectra to graft dynamics a variable temperature study was undertaken (Fig. 2). Spectra were

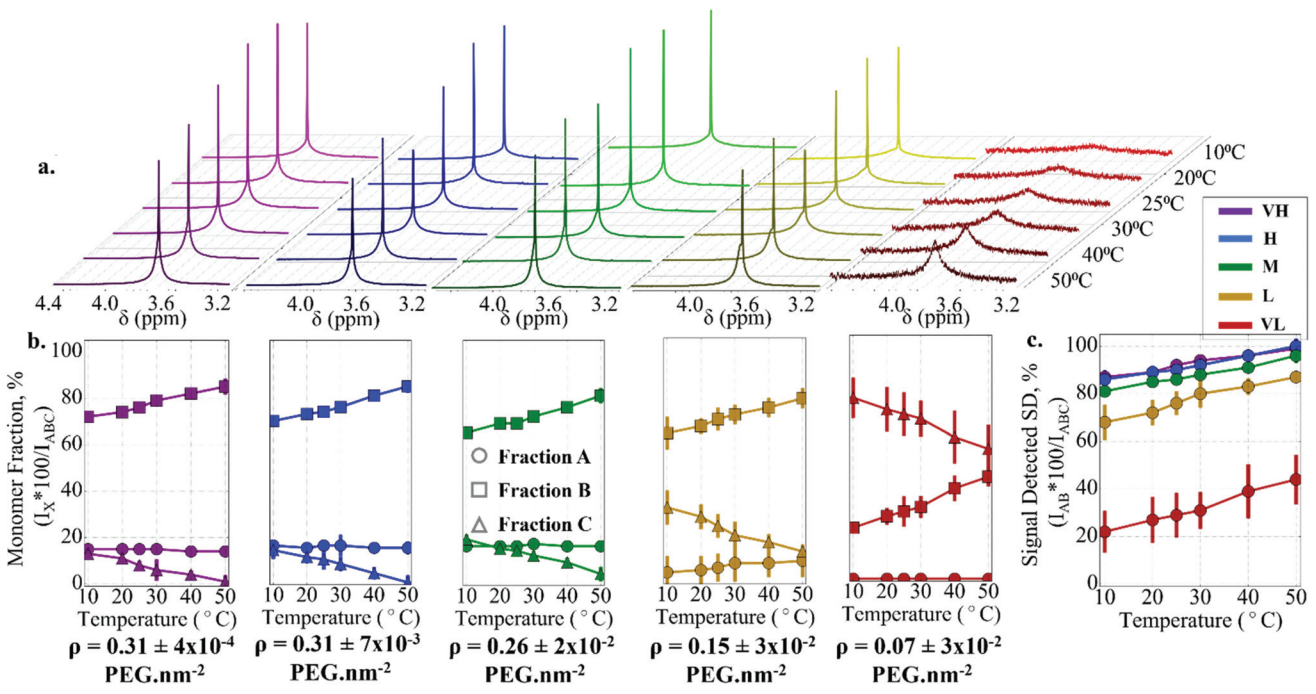

Fig. 2 Analysis of the temperature dependence of the 1H spectra for different surface coverage. (a) Representative example of the temperature dependence of the ^{1}H NMR spectra recorded for a batch of VH to VL suspensions of PEG_{5000}-grafted 50 nm SiO_2 NPs. (b) Temperature dependence of the monomer distribution into fractions *A*, *B* and *C* (quantified using the 3 Lorentzian model), averaged for the spectra shown in (a) and two other independent samples. The average (*n* = 3 batches) PEG coverage is noted below each graph. Error bars are indicative of the standard deviation. (c) Temperature dependence of the signal detected (SD = IAB × 100/IABC), note that PEG_{5000} has an average of 114 units.

Published on 22 February 2021. Downloaded by TU Dublin on 4/4/2022 10:07:53 AM.

recorded every 10 °C following temperature equilibration. The residual water peak was used to confirm the sample temperature and temperature stability. The spectra in Fig. 2 were measured as soon as possible after synthesis, in this case in the same week, to avoid long term surface stability issues. The curves in Fig. 2b and c are the averages of 3 independent particle batches synthesised side-by-side on the same day. The experiment was also repeated with a multitude of samples at different stages during the study with comparable results.

A gradual increase in intensity and narrowing of the high resolution ethylene glycol signal with increasing temperature or coverage are observed (Fig. 2a). Quantification of the fractions by line-fitting (I_A, $I_{B''}$ *and* $I_{B''}$) and evaluation of their relative contribution to the total signal (I_{ABC}), reveals that for all suspensions there is a gradual transfer of ^{1}H signal intensity from fraction *C* to *B* and from *B* to *A* (Fig. 2b) with increasing coverage and with increasing temperature. We ascribe both trends to gradual reduction in residual dipolar interactions (averaged to zero giving sharp spectra in the case of ethylene glycol units in the fast-motion limit) associated with faster chain dynamics for an increasing number of monomers along the chains, *i.e.* chain mobility increases with temperature. Physically this may correspond to a shift of the ethylene glycol units average positions away from the surface. Consequently this model suggests less extended average chain conformations at low ρ which is in line with the de Gennes model.[63] The transfer of ^{1}H magnetisation between fractions is more consistent with fairly uniform coverage throughout the suspension as opposed to the presence of sub-populations of particles with different coverage. This interpretation is supported by hole-burning experiments conducted for all coverages (Fig. S13†), which show that it is not possible to burn a hole in fraction *B*, demonstrating that it is predominantly homogeneously broadened. Presumably this is due to residual dipolar interactions (see ESI†) associated with conformational restraints.

To quantify the non-detectable ^{1}H magnetisation (fraction *C*) we calculate the % of the ethylene glycol units signal detectable in the suspension as SD = $(I_{AB}/I_{ABC}) \times 100$. The temperature and coverage dependence of SD are revealing (Fig. 2c). At 25 °C the SD value for **VH**, **H** and **M** particles is between 85 and 90% while for **L** and **VL** it is significantly lower, at ~75% and ~25% respectively. Hence at lower coverage only a small fraction of the ethylene glycol units are sufficiently mobile to be detectable. Increasing temperature resulted in an increase in SD for all coverages (notably to *c.*100% for **VH**), corresponding to a transfer of units from fraction *C* to *B* (increasing I_{AB}). A relatively small change in SD was observed for particles with high to moderate ligand coverage, **VH** 13%, **H** 14% and **M** 15%, when the temperature was increased from 10 to 50 °C. However, low ρ resulted in a larger transfer for **L** of 20% (from 68 to 87%) and for **VL** 22% (22 to 44%), *i.e.* to a greater fraction of the units moving into the faster motion regime. These findings are consistent with results for PEG_{1000} for different particle sizes, where the resonance ceases to be observable below a certain surface coverage which depends on the particle size (Fig. S8d–f, Table S1† and Fig. 4 in our previous work[29]).

A more rigorous analysis of fractions *A* and *B* reveals an increase in both I_A and I_B with temperature where the relative increase in the latter is larger. That is more units are transferred from *C* to *B* than from *B* to *A*, and both observable features narrow on increasing temperature (Fig. 2a and S14†). For example, the FWHM of *B* of **VH** suspensions decreased from ~80 to ~30 Hz on increasing the temperature from 10 to 50° C. The width of *A* increased marginally from ~1.8 to ~2.3 Hz in the same range. Comparable behavior was observed for **H** and **M** dispersions (Fig. 2a, b and S14†). Interestingly, we also observe subfractions of *A* at higher temperatures (40–50 °C, Fig. S15†), a change that is reversible on cooling back down. Finally, **L** and **VL** dispersions were found to behave differently. In the case of the former the line-shape of the peak was more apparently bimodal, specifically fraction *B* was shifted more downfield than in higher ligand coverage particles (Fig. S16†). While **VL** did not exhibit a narrow fraction, even at elevated temperature. Additionally the number of Lorentzian components used in the line-fitting had to be reduced from two to one for **VL** particles at low temperatures.

In summary the trends of an increase in SD (Fig. 2c), a reduction in FWHM (Fig. 2a and S9†) and a shift upfield on increasing temperature were observed for all sample batches and all coverages, changes which are consistent with increasing chain mobility. These systematic changes, and in particular the temperature-dependence of SD as a function of ligand coverage (Fig. 2c), were more pronounced at lower ρ (**L** and **VL**). Interestingly, total batch-to-batch variability in the line-shape and resulting quantification were greatest for **L**, indicating that the dynamics changes sharply in this ρ range. As noted above the observed trends were independent of the fitting model used (this is demonstrated in Fig. S17†).

Ligand mobility and ^{1}H NMR relaxometry

The interpretation of the changes in the spectra with particle and ligand size (Fig. 1), temperature (Fig. 2) and ligand coverage as arising from changes in ligand mobility and possibly conformation were further evaluated using ^{1}H NMR relaxometry. Spin–lattice, T_1, and spin–spin, T_2, relaxation times were measured (details in ESI†) for the PEG resonance in **VH**, **H**, **M** and **L** suspensions, between 10 and 50 °C. **VL** could not be studied due to low signal intensity at achievable NP concentrations. Dephasing times, $T^{FW}_{2L,S}$, were calculated from the spectral lineshape analysis as $T^{FW}_{2L,S} = 1/\pi\nu_{FWHM}$, where ν_{FWHM} is the full width at half maximum extracted for each fraction.

The PEG T_1 values were found to be in the range of 750–1400 ms with only minor differences observed between the values for fractions *A* and *B* at 25 °C (Fig. S19†). Spectra recorded with the inversion recovery sequence confirm the complete absence of any fast T_1 relaxation in the ms range (Fig. S20–22†). The T_1 values were weakly dependent on coverage in the measured temperature range. The values for fraction *B* increased slightly, by ~17%, and for fraction *A* more significantly, by ~120%, between 10 and 50 °C (Fig. S19a, b and Table S3†) demonstrating that both fractions are in the fast motion regime. As a relaxation minimum was not present in

 This journal is © The Royal Society of Chemistry 2021

Published on 22 February 2021. Downloaded by TU Dublin on 4/4/2022 10:07:53 AM.

the available temperature window application of a model to interpret the dynamics incurs uncertainties and so is not presented.

In contrast the PEG T_2 relaxation was found to have two distinct stages (Fig. S23†) and to be more sensitive to dynamical restrictions of interest. A short process with T_{2S} of up to 15 ms, and a long one with $T_{2L} \geq 2000$ ms for full recovery were always observed (Fig. S24†). Changes in the spectral shape during the echo train show that the fast and slow decays arise from fractions *B* and *A*, respectively (Fig. S23b†). For both fractions T_2 increased with temperature (Fig. 3a and b). Details of the approach used to extract T_2 values are provided in Fig. S25 and Table S2.†

The T_{2L} values (fraction *A*) are less interesting as these ethylene glycol units are hardly affected by graft restrictions. As the T_{2L} values were very similar to T_1 we can conclude this fraction is indeed in the motional averaging regime ($T_1 \approx T_2$). This is typical for low molecular weight species undergoing rapid isotropic motion. It is worth while noting that the T_{2L} recorded for fraction *A* is similar to the T_2 value of free PEG, there is a small measurable difference (Fig. 3a). For completeness, the T_{2L} values were slightly longer than the T_{2L}^{FW} values from lineshape analysis (Fig. S26†), suggesting some heterogeneous contributions to the broadening of *A*. This is most likely due to field inhomogeneity, which is supported by broadening of resonances from low molecular weight species in the suspension (*e.g.* internal standard DMF, Fig. S27†).

The PEG T_{2S} values were two orders of magnitude smaller and interestingly they were found to be somewhat dependent on temperature, coverage, PEG length and particle size. From the good correlation between T_{2S} and T_{2S}^{FW} (Fig. S28†) and the fact that hole-burning is not possible we can conclude that this ^{1}H magnetisation fraction is homogeneously broadened. This confirms that the spectral features (Fig. 1 and 2) arise from different dynamic fractions of ethylene glycol units and not from particle subfractions. We will use the T_{2S} (rather than the T_{2S}^{FW}) values for data interpretation which are extracted using 300 echoes rather than a single FWHM and are thus considered more accurate (details in ESI, Fig. S28†).

Independently increasing either the temperature or the coverage (Fig. 3b) lead to an increase of T_{2S}, strongly suggesting that either change activates the dynamic process driving the relaxation. Similar behavior was observed using 65 nm SiO_2 particles (Fig. S29†).

The dependence of T_{2S} on ρ was further explored through partial dissolution of **VH** particles in low salinity media, *i.e.* surface etching (Fig. 3c). This treatment led to a reduction in coverage of 0.08 PEG per nm (36%) with no measurable change in gross sample morphology (Fig. 3f), hydrodynamic size or colloidal stability (Fig. S30a†). Final ligand coverage was similar to that of **L** particles. The change in PEG surface coverage over this time was measurable by NMR (Fig. 3d), and free PEG was subsequently found in the supernatant (Fig. S30b†). As expected the etching process led to a reduction in the measured T_{2S} values for the particles at all temperatures (Fig. 3e), indeed these values were found to be between those

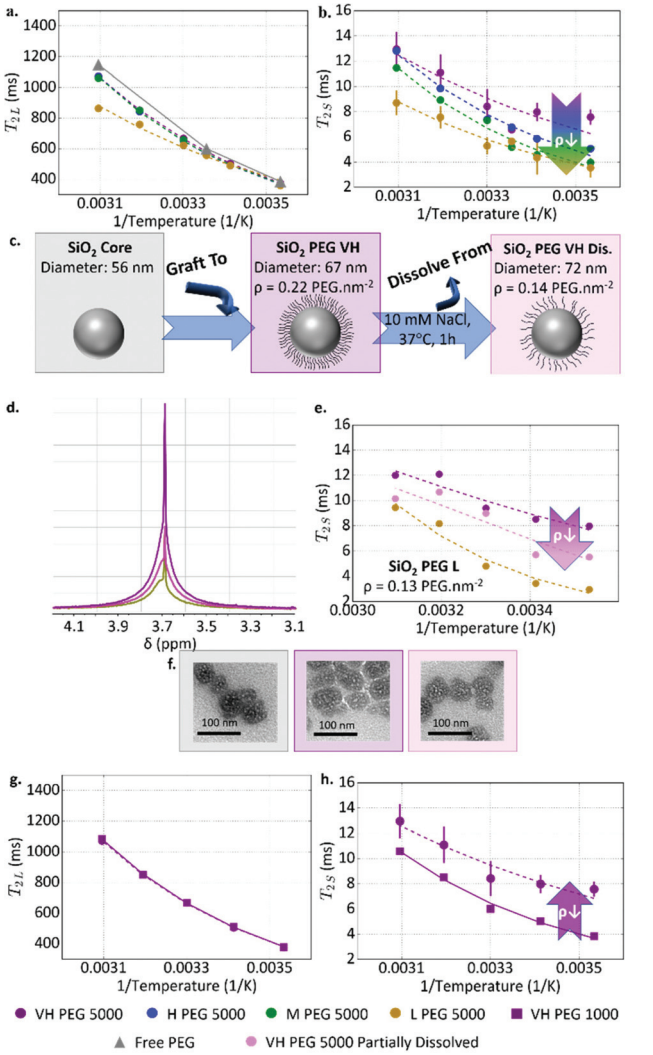

Fig. 3 Dependence of spin–spin relaxation on coverage, particle size and temperature. ^{1}H relaxometric analysis for (a) T_{2L} and (b) T_{2S} as a function of temperature for 50 nm PEG_{5000}-grafted NP suspensions of different coverage, compared to free PEG (grey triangles). Data presented in (a) and (b) is the average for n = 3 samples. (c) Schematic representation of the particle grafting and controlled particle dissolution. (d) Reduction of ^{1}H signal for 50 nm NP suspensions before (purple) and after (magenta) partial dissolution. (f) TEM showing the absence of substantial morphological change over the same stages shown in (c). (e) T_{2S} of 50 nm PEG_{5000} grafted **VH** particles (ρ = 0.22 nm^{-2}) and surface diluted **VH** particles (ρ = 0.14 nm^{-2}) compared with **L** particles (ρ = 0.13 nm^{-2}). (g) T_{2L} and (h) T_{2S} recorded for the same 50 nm NP suspension grafted with PEG_{5000} (ρ = 0.35 nm^{-2}, **VH**, purple circles) and PEG_{1000} (ρ = 0.9 nm^{-2}, purple squares). The dashed lines represent fits to the data (see methods). The T2L trend for **VH**, **H** and **M** particles in (a) and PEG_{1000} and PEG_{5000} in (g) overlap completely and are thus difficult to distinguish in the figure.

of the **VH** and **L** suspensions. A similar effect of reducing T_{2S} was also found on prolonged storage in D_2O at RT, with the associated increase of free PEG also confirmed.

The effects of reducing chain length are shown in Fig. 3g and h for 50 nm NPs grafted with PEG_{5000} (ρ 0.35 nm^{-2}) and

Published on 22 February 2021. Downloaded by TU Dublin on 4/4/2022 10:07:53 AM.

PEG_{1000} (ρ 0.9 nm^{-2}). The T_{2L} value was found to be insensitive to the chain length indicating that the dynamics of *A* are largely unchanged. I_A/I_B decreased for shorter chains consistent with fewer unhindered units in fraction *A*, as expected, and T_{2s} decreased suggesting more hindered dynamics for fraction *B*.

Hence over the range of particle size, coverage and chain length studied, NMR relaxometry and spectral analysis demonstrate increasing numbers of ethylene glycol units move from less to more dynamic fractions. This suggests that the fraction of the grafts in the different dynamic regimes can be precisely controlled through surface graft coverage and modification.

Effect of ligand coverage in complex media

The NMR analysis (FWHM and total intensity) suggests strong coverage dependent changes between **H**/**L** and between **L**/**VL** suspensions. This is especially clear in Fig. 1 where a ~30% reduction in coverage leads to a nearly threefold reduction in intensity. Changes in graft dynamics may result in changes to the colloidal stability and other responses; hence aggregation studies in media of increasing salinity and protein binding studies were undertaken.

The dependence of colloidal stability at different ionic strength (IS) on PEG coverage was measured by DLS salt titration (Fig. S31† shows data for three independent particle batches). It was found that suspensions of 50 nm NPs were more stable to increasing IS at either extreme of the PEG_{5000} coverage range studied. Specifically, the higher ρ dispersions (**VH** and **H**) exhibited good colloidal stability up to 100 mM (NaCl in PBS) as did **VL**. It is important to note that bare silica particles are stable in the test conditions. However, suspensions of intermediate coverage particles, *i.e.* **M** and **L**, destabilised at 20 and 40 mM, respectively. Detailed analysis on the mechanism of the coverage dependent aggregation is beyond the scope of this work. However, loss of steric stabilisation at intermediate ρ is apparent and at very low coverage the surface behaves more like free (electrostatically stabilised) silica NPs.

Protein binding of the particles was evaluated by incubating 50 nm SiO_2 PEG_{5000} suspensions with undiluted human serum in a 1 to 1 volume ratio for an hour, stationary at RT. After this time dispersions were washed four times to remove free proteins. A continual increase of bound protein was observed, by microBCA and gel silver staining, over the **VH** to **L** range (Fig. S32a and d†). The largest increases (~80% of the total protein bound) occurred from **H** to **M** and from **M** to **L**, representing a jump of 0.14 and 0.17 mg mL^{-1}, respectively. Increased protein binding with reducing PEG coverage is well documented.[3,64–66] We note here for the first time a correlation between protein binding and a shift in ligand dynamics (revealed by NMR), and in particular the strong negative correlation between binding and SD (% of the ethylene glycol units detectable by ^{1}H NMR) at 25 °C. Note also that suspensions with intermediate coverage (**M** and **L**) are not stable when incubated with human serum, as may be expected from the results above (Fig. S32b†). The composition of the hard protein corona, obtained from full human serum, was also found to change with PEG surface coverage, for **VH** and **H** it was composed mostly of proteins in the 46–58 kDa (~40%) and 58–80 kDa ranges (~20%). For lower coverage the molecular weight distribution was broader, and that was particularly the case for **VL** for which the distribution was similar to that for uncoated SiO_2 (Fig. S32c and d†). The detailed molecular interactions giving rise to these observations are an interesting question but beyond the scope of this work; but again we note the correlation between ligand dynamics measured by NMR and corona composition.

Discussion

In summary ^{1}H NMR analysis of the suspensions identifies three signal fractions: *A* which is similar to free PEG in terms of width (FWHM 1–4 Hz) and T_1/T_2 relaxation times on the order of several seconds. It arises from relatively mobile ethylene glycol units. *B* which is broader (13–300 Hz) with T_2 of the order of several microseconds and δ between 3.69 and 3.73 ppm. It arises from units which experience significant conformational restraints, presumably due to proximity to the particle surface. Finally, *C* which is broadened into the background. It arises from units which are closest to the surface and are in slow motion on the NMR timescale. The physical picture that emerges is shown schematically in Fig. 4a.

The spectral analysis poses the question of whether *A* arises from the highly mobile units of bound chains alone or if there are also contributions from free PEG and/or unbound but entangled polymer. As noted above, initially the free PEG found in the last supernatant is negligible. The reversible formation at elevated temperature of subfractions of *A*, the stability of the spectra (shown in Fig. 2) over the two week timeframe of the analysis, and the reproducibility of the analysis in Fig. 2 for other preparations (see ESI†) which were recorded at different times within their two week window demonstrate that *A* arises largely from bound PEG. This is further supported by the small difference in T_2 between *A* and free PEG (Fig. 3a). Hence while the I_A values may be slightly overestimated the reversible temperature-dependent changes in the population of the fractions arise from changes in on-particle graft dynamics. Zhang *et al.* used DOSY spectroscopy to assign bound and free ligand resonances, for 17.5 kDa poly(allylamine) grafted 5 nm nanodiamonds, based on their diffusion coefficients.[51] We were unable to use DOSY for quantitation due to the significant spectral overlap in the region of interest complicated by minor gradient induced distortions of the lines.

Ethylene glycol units are found to move between fractions on changing temperature. Increasing from 10 to 50 °C results in transfer from *C* to *B* and from *B* to *A* which are reversible on cycling the temperature (Fig. S33†). This is manifested by more signal becoming measurable (*i.e.* a reduction of fraction *C*), and the resonance narrowing (by tens of Hz), both due to increased chain mobility arising from reduced interactions with the particle surface as confirmed by T_2 relaxometry, as schematically presented in Fig. 4a. Similar coverage dependent effects are observed for different particle sizes and chain

 This journal is © The Royal Society of Chemistry 2021

Published on 22 February 2021. Downloaded by TU Dublin on 4/4/2022 10:07:53 AM.

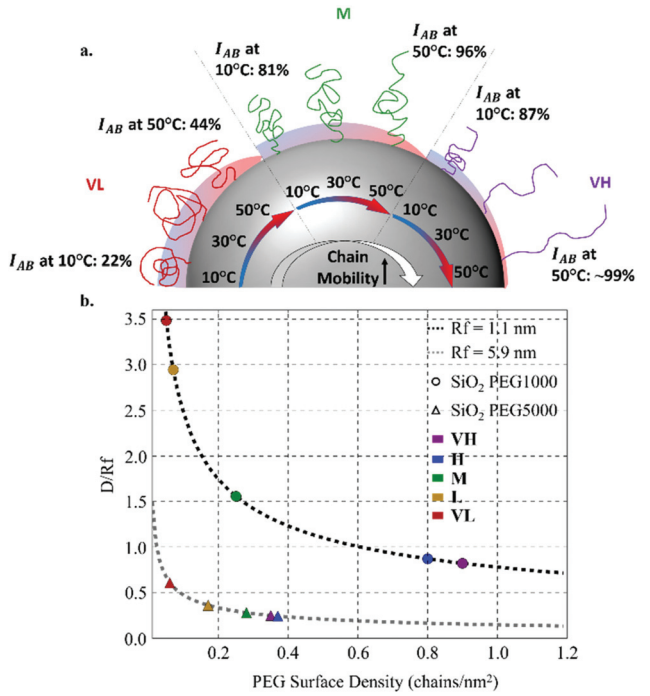

Fig. 4 Evolution of the dynamic domain populations and proposed interpretation models. (a) Proposed conformational changes of the PEG_{5000} ligand with an increase in temperature and surface coverage. Blue-red areas at the bottom of the ligand reflect shifts in signal recovery. Chain mobility is observed by peak FWHM in NMR. (b) Calculated ratio of the average distance between PEG chains to their Flory radius, as a function of ligand surface coverage for both PEG lengths used.

lengths. Conversely transfer of units from *B* to *C* can be achieved by reducing temperature or by removing surface silanised PEG by dissolution (Fig. 4a).

Ligand conformation and the average distance to the surface, which we suggest determine dynamics underpinning the NMR response, are predicted by the Alexander–de Gennes model.[12,42,63] The ratio between the average ligand-to-ligand distance (D) and the Flory radius (R_f) is often used to classify ligand surface conformation, though the exact cutoffs are not agreed. Generally for $D/R_f < 1$ the chains are considered to be in a brush conformation, while $D/R_f > 2$ results in a mushroom conformation.[34,60,63,66,67] D/R_f values calculated for the SiO_2 PEG_{5000} samples are in the brush conformation regime (Fig. 4b). Thus our model suggests that for 50 nm particles there is a relatively smooth change in properties between a dense brush, *i.e.* **VH** and **H** particles, to intermediate stages (**M** and possibly **L**) to a loose brush, **VL**. This demonstrates firstly that the detectable ^{1}H signal corresponds to surface distant parts of the chains in a relatively dense brush conformation. Secondly, it is interesting that the D/R_f values are correlated with the extent of protein binding (Fig. S32a and S34†), *i.e.* particles with low D/R_f (or high ρ) tend to bind less protein in both microBCA and SDS-PAGE experiments.

The relationship between protein binding and ligand coverage has been well documented.[3,29,67] This behaviour has previously been linked to the potential loss of ligand entropy and to disruption of a structured water layer at the particle surface, which is energetically unfavorable.[39,66–67] However, to our knowledge, this is the first time ligand conformation as measured by NMR, and indexed with D/R_f values, has been correlated with protein concentration in the hard corona (Fig. S34†).

The work presented here provides a more detailed microscopic picture of the dynamic ligand derived aspects of these key surface phenomena. New questions about the factors that determine fraction population arise when our observations are considered with other reports in literature,[42,51] where chain mobility is estimated through NMR. For instance the above noted study from Zhang *et al.*[51] suggested that based on relaxometry 45% of the polymer retains rapid motion. This is far greater than what we observe and may be due to the smaller particle size and increased curvature. Interestingly Wu *et al.* report that ligand coverage decreases as particle size is increased[42] which our data confirms (Table S1†). Importantly in both studies NP-ligand grafting leads to peak broadening when the same ligand is bound to particles with increasing size (Fig. 1d).

Conclusions

The surface PEG coverage and temperature induced changes in ^{1}H NMR lineshape and relaxation times are explained by differences in ligand mobility due to slowing of chain motions. Reduced mobility is associated with proximity to the particle surface and not from inter-chain steric hindrance, *i.e.* mobility increases with coverage. On transition from high (**VH**, **H**) to intermediate (**M**, **L**) to low (**VL**) coverage significant changes in the ^{1}H response, the colloidal stability with salt titration and in the serum protein binding (total and distribution) were observed which are consistent with ligand conformational transitions from dense to looser brush. This work and the related literature[42,51] demonstrate the central roles of the particle-to-ligand size ratio and ligand coverage in these changes.

Preliminary NMR analysis of PEGylated particles in a protein solution posed a significant challenge due to overlap in the ethylene glycol region of the spectrum. Thus here we describe the situation for the protein-free surfaces at which the initial recognition events must occur. This work provides a framework to investigate graft coverage dependence of protein binding and so is a step towards better understanding of the molecular processes on PEGylated nanoparticle surfaces that determine their biological response. An interesting question that arises is the link between ligand mobility, protein residence time and recognition, which may be addressable for single protein exposures. We suggest that the effect of surface coverage and distribution of dynamic ethylene glycol units on protein interactions demonstrated here will be shown to play a key role in the processes that determine recognition in the low binding affinity scenario under biologically-relevant conditions.

Published on 22 February 2021. Downloaded by TU Dublin on 4/4/2022 10:07:53 AM.

Experimental section

Methods not reported here can be found in the accompanying ESI section.†

50 nm SiO_2 particle synthesis and modification

FITC – APTMS conjugation. The labelling conjugate was prepared prior to particle synthesis by dissolving 2 mg of fluorescein isothiocyanate (FITC) in 1 mL of ethanol (99.9%) to which 10 μL of (3-Aminopropyl)triethoxysilane (APTMS) were added. The reaction was covered with aluminium foil and left to react for a minimum of 4 hours at 20 °C. A 2 mL Eppendorf tube was used in all cases.

Nanoparticle synthesis. Silica particles were synthesised using a slight modification of the Stöber method.[29] 0.91 g of ammonia (28.0–30.0% NH_3 basis) was added to 25 mL of ethanol (99.9%) in a 50 mL polypropylene container. To which 0.5 mL of the prepared FITC-APTMS conjugate solution (see above) were pipetted. The reaction was stirred for 1 minute, upon which Tetraethyl orthosilicate (0.94 ml) was added. The reaction was then stirred at 600 rpm at 20 °C for a further 20 hours in darkness. The resulting nanoparticle suspension was centrifuged down at 13 500 rpm for 20 minutes. The pellet was resuspended in fresh ethanol once and water three further times using bath sonication.

PEGylation of 50 nm silica nanoparticles. 1 mL of 5–10 mg mL^{-1} silica particles were preheated to 90 °C and allowed to equilibrate for 10 minutes while shaking at 6000 rpm. 5 kDa and 1 kDa methylated PEG silicate were added to the particles in a concentration of 5 (VH), 2.5 (H), 1 (M), 0.2 (L) and 0.015 (VL) PEG per nm^2. The dispersions were left to react in this way for one hour after which they were washed with water twice and deuterium oxide two further times as described in section 2.2 for 50–100 nm particles and section 2.4 for 200 nm ones. Trimethylamine was used to augment the pH to 9 for experiments reported in Fig. S6.†

Particle characterisation

Size by dynamic light scattering (DLS). A Malvern Zetasizer ZS series was used in all measurements. Bare and PEGylated silica particles were diluted in water as 1 in 100 for a final concentration of ~100 μg mL^{-1} in a plastic low volume cuvette (PLASTIBRAND, semi-micro, PMMA, l = 1 cm). Each measurement was conducted at least three times and consisted of 11 consecutive 10 s runs at 25 °C. There was no equilibration time prior to experiment.

Temperature stability by DLS (data not shown). Temperature trends were conducted in the DLS in the range of 10–50 °C measuring every 10 °C with an equilibration time of 20 minutes. Each point consisted of 10 consecutive runs.

^{1}H NMR spectroscopy

Sample preparation for NMR. If the washed particles were dispersed in H_2O they were spun at 13 500 rpm for 15 min and redispersed in D_2O 1 mM DMF after supernatant removal and with the assistance of bath sonication. This procedure was repeated once more. Both the last supernatant and final particle dispersion were kept.

^{1}H NMR using varian VNMRs 400 MHz. 1 mL of particles (>5 mg mL^{-1}) in D_2O 1 mM DMF were pipetted into a 5 mm thin wall, 8 inch NMR tube (Wilmad Lab Glass) and placed in the instrument. Each measurement was conducted at room temperature with a 45° pulse and 6 scans with a relaxation delay of 25 seconds.

^{1}H NMR using varian VNMRs 600 MHz. 0.7 mL of particles (>5 mg mL^{-1}) in D_2O 1 mM DMF were pipetted into a 5 mm thin wall, 8 inch NMR tube (Wilmad Lab Glass) and placed in the instrument. The PROTON was run with a hard 45 degrees 1H pulse of duration 3.20 us, relaxation delay of 25 s, acquisition time of 5.0 s, number of scans of 16, TOF at −215.95 Hz (4.64 ppm), processing with 48 K points and no weighting function applied before the Fourier Transformation.

Fitting 1H spectra. NMR signals were fit using a mixture of models including a single Gaussian and Lorentzian function, 2, 3 and 4 Gaussians and Lorentzians, as well as several combinations of types. The R2 and fraction of the signal fitted were calculated and used as measures of the fit quality. The fitting model was chosen based on the fewest number of parameters required to best fit the signal which was three Lorentzian peaks. The R2 and signal fraction fit of was >0.99 in every case. It was shown that Lorentzian fits are more appropriate than Gaussians through analysing the fitting moments. See section "Details on lineshape analysis" above for more details.

Author contributions

DRH conceived, designed and executed studies, drafted and corrected the paper. HL conceived studies and led fitting studies. YO designed and ran NMR experiments. KS executed studies. KD conceived studies, drafted and corrected the paper. DB conceived and designed studies, drafted and corrected the paper.

Conflicts of interest

The authors have no conflicts to declare.

Acknowledgements

K. A. D. acknowledges that this publication has emanated from research supported in part by a grants from Science Foundation Ireland (17/NSFC/4898 and 17/ERCD/4962). The team would like to thank Prof. Kimberly Hamad-Schifferli for assistance with the manuscript.

Notes and references

1 D. Kwon, J. Park, J. Park, S. Y. Choi and T. H. Yoon, Effects of surface-modifying ligands on the colloidal stability of ZnO nanoparticle dispersions in in vitro cytotoxicity test media, *Int. J. Nanomed.*, 2014, **9**(Suppl. 2), 57.

 This journal is © The Royal Society of Chemistry 2021

Published on 22 February 2021. Downloaded by TU Dublin on 4/4/2022 10:07:53 AM.

2 S. J. Sofia, V. Premnath and E. W. Merrill, Poly (ethylene oxide) grafted to silicon surfaces: grafting density and protein adsorption, *Macromolecules*, 1998, **31**(15), 5059–5070.
3 N. Bertrand, P. Grenier, M. Mahmoudi, E. M. Lima, E. A. Appel, F. Dormont, J.-M. Lim, R. Karnik, R. Langer and O. C. Farokhzad, Mechanistic understanding of in vivo protein corona formation on polymeric nanoparticles and impact on pharmacokinetics, *Nat. Commun.*, 2017, **8**(1), 777.
4 C. Rodriguez-Quijada, M. Sánchez-Purrà, H. de Puig and K. Hamad-Schifferli, Physical Properties of Biomolecules at the Nanomaterial Interface, *J. Phys. Chem. B*, 2018, **122**(11), 2827–2840.
5 S. Schöttler, G. Becker, S. Winzen, T. Steinbach, K. Mohr, K. Landfester, V. Mailänder and F. R. Wurm, Protein adsorption is required for stealth effect of poly (ethylene glycol)-and poly (phosphoester)-coated nanocarriers, *Nat. Nanotechnol.*, 2016, **11**(4), 372.
6 P. Aggarwal, J. B. Hall, C. B. McLeland, M. A. Dobrovolskaia and S. E. McNeil, Nanoparticle interaction with plasma proteins as it relates to particle biodistribution, biocompatibility and therapeutic efficacy, *Adv. Drug Delivery Rev.*, 2009, **61**(6), 428–437.
7 J. L. Perry, K. G. Reuter, M. P. Kai, K. P. Herlihy, S. W. Jones, J. C. Luft, M. Napier, J. E. Bear and J. M. DeSimone, PEGylated PRINT nanoparticles: the impact of PEG density on protein binding, macrophage association, biodistribution, and pharmacokinetics, *Nano Lett.*, 2012, **12**(10), 5304–5310.
8 J. Cui, R. De Rose, K. Alt, S. Alcantara, B. M. Paterson, K. Liang, M. Hu, J. J. Richardson, Y. Yan and C. M. Jeffery, Engineering poly (ethylene glycol) particles for improved biodistribution, *ACS Nano*, 2015, **9**(2), 1571–1580.
9 P. Falagan-Lotsch, E. M. Grzincic and C. J. Murphy, One low-dose exposure of gold nanoparticles induces long-term changes in human cells, *Proc. Natl. Acad. Sci. U. S. A.*, 2016, **113**(47), 13318–13323.
10 G. Maiorano, S. Sabella, B. Sorce, V. Brunetti, M. A. Malvindi, R. Cingolani and P. P. Pompa, Effects of cell culture media on the dynamic formation of protein–nanoparticle complexes and influence on the cellular response, *ACS Nano*, 2010, **4**(12), 7481–7491.
11 R. Rietscher, M. Schröder, J. Janke, J. Czaplewska, M. Gottschaldt, R. Scherließ, A. Hanefeld, U. S. Schubert, M. Schneider and P. A. Knolle, Antigen delivery via hydrophilic PEG-b-PAGE-b-PLGA nanoparticles boosts vaccination induced T cell immunity, *Eur. J. Pharm. Biopharm.*, 2016, **102**, 20–31.
12 T. Drobek, N. D. Spencer and M. Heuberger, Compressing PEG Brushes, *Macromolecules*, 2005, **38**(12), 5254–5259.
13 X. Liu, H. Tao, K. Yang, S. Zhang, S.-T. Lee and Z. Liu, Optimization of surface chemistry on single-walled carbon nanotubes for in vivo photothermal ablation of tumors, *Biomaterials*, 2011, **32**(1), 144–151.
14 Z. Liu, C. Davis, W. Cai, L. He, X. Chen and H. Dai, Circulation and long-term fate of functionalized, biocompatible single-walled carbon nanotubes in mice probed by Raman spectroscopy, *Proc. Natl. Acad. Sci. U. S. A.*, 2008, **105**(5), 1410–1415.
15 G. Prencipe, S. M. Tabakman, K. Welsher, Z. Liu, A. P. Goodwin, L. Zhang, J. Henry and H. Dai, PEG branched polymer for functionalization of nanomaterials with ultralong blood circulation, *J. Am. Chem. Soc.*, 2009, **131**(13), 4783–4787.
16 M. Colombo, L. Fiandra, G. Alessio, S. Mazzucchelli, M. Nebuloni, C. De Palma, K. Kantner, B. Pelaz, R. Rotem and F. Corsi, Tumour homing and therapeutic effect of colloidal nanoparticles depend on the number of attached antibodies, *Nat. Commun.*, 2016, **7**, 13818.
17 Y. Bao, E. Guégain, J. Mougin and J. Nicolas, Self-stabilized, hydrophobic or PEGylated paclitaxel polymer prodrug nanoparticles for cancer therapy, *Polym. Chem.*, 2018, **9**(6), 687–698.
18 N. Mackiewicz, J. Nicolas, N. G. Handké, M. Noiray, J. Mougin, C. Daveu, H. R. Lakkireddy, D. Bazile and P. Couvreur, Precise engineering of multifunctional PEGylated polyester nanoparticles for cancer cell targeting and imaging, *Chem. Mater.*, 2014, **26**(5), 1834–1847.
19 J. J. Mittag, B. Kneidl, T. Preiβ, M. Hossann, G. Winter, S. Wuttke, H. Engelke and J. O. Rädler, Impact of plasma protein binding on cargo release by thermosensitive liposomes probed by fluorescence correlation spectroscopy, *Eur. J. Pharm. Biopharm.*, 2017, **119**, 215–223.
20 Z. Ban, P. Yuan, F. Yu, T. Peng, Q. Zhou and X. Hu, Machine learning predicts the functional composition of the protein corona and the cellular recognition of nanoparticles, *Proc. Natl. Acad. Sci. U. S. A.*, 2020, **117**(19), 10492–10499.
21 R. Cai, J. Ren, Y. Ji, Y. Wang, Y. Liu, Z. Chen, Z. Farhadi Sabet, X. Wu, I. Lynch and C. Chen, Corona of Thorns: The Surface Chemistry-Mediated Protein Corona Perturbs the Recognition and Immune Response of Macrophages, *ACS Appl. Mater. Interfaces*, 2019, **12**(2), 1997–2008.
22 P. M. Kelly, C. Åberg, E. Polo, A. O'Connell, J. Cookman, J. Fallon, Ž Krpetić and K. A. Dawson, Mapping protein binding sites on the biomolecular corona of nanoparticles, *Nat. Nanotechnol.*, 2015, **10**(5), 472.
23 M. C. L. Giudice, L. M. Herda, E. Polo and K. A. Dawson, *In situ* characterization of nanoparticle biomolecular interactions in complex biological media by flow cytometry, *Nat. Commun.*, 2016, **7**, 13475.
24 M. P. Monopoli, C. Åberg, A. Salvati and K. A. Dawson, Biomolecular coronas provide the biological identity of nanosized materials, *Nat. Nanotechnol.*, 2012, **7**(12), 779.
25 M. Steinke, F. Zunhammer, E. I. Chatzopoulou, H. Teller, K. Schütze, H. Walles, J. O. Rädler and C. Grüttner, Rapid Analysis of Cell–Nanoparticle Interactions using Single–Cell Raman Trapping Microscopy, *Angew. Chem., Int. Ed.*, 2018, **57**(18), 4946–4950.
26 M. Carril, D. Padro, P. del Pino, C. Carrillo-Carrion, M. Gallego and W. J. Parak, In situ detection of the protein corona in complex environments, *Nat. Commun.*, 2017, **8**(1), 1542.

Published on 22 February 2021. Downloaded by TU Dublin on 4/4/2022 10:07:53 AM.

27 T. Miclăuş, C. Beer, J. Chevallier, C. Scavenius, V. E. Bochenkov, J. J. Enghild and D. S. Sutherland, Dynamic protein coronas revealed as a modulator of silver nanoparticle sulphidation in vitro, *Nat. Commun.*, 2016, **7**, 11770.

28 T. L. Moore, L. Rodriguez-Lorenzo, V. Hirsch, S. Balog, D. Urban, C. Jud, B. Rothen-Rutishauser, M. Lattuada and A. Petri-Fink, Nanoparticle colloidal stability in cell culture media and impact on cellular interactions, *Chem. Soc. Rev.*, 2015, **44**(17), 6287–6305.

29 D. R. Hristov, L. Rocks, P. M. Kelly, S. S. Thomas, A. S. Pitek, P. Verderio, E. Mahon and K. A. Dawson, Tuning of nanoparticle biological functionality through controlled surface chemistry and characterisation at the bioconjugated nanoparticle surface, *Sci. Rep.*, 2015, **5**, 17040.

30 A. Salvati, A. S. Pitek, M. P. Monopoli, K. Prapainop, F. B. Bombelli, D. R. Hristov, P. M. Kelly, C. Åberg, E. Mahon and K. A. Dawson, Transferrin-functionalized nanoparticles lose their targeting capabilities when a biomolecule corona adsorbs on the surface, *Nat. Nanotechnol.*, 2013, **8**(2), 137.

31 P. S. Naidu, M. Norret, N. M. Smith, S. A. Dunlop, N. L. Taylor, M. Fitzgerald and K. S. Iyer, The Protein Corona of PEGylated PGMA-Based Nanoparticles is Preferentially Enriched with Specific Serum Proteins of Varied Biological Function, *Langmuir*, 2017, **33**(45), 12926–12933.

32 R. Rial, B. Tichnell, B. Latimer, Z. Liu, P. V. Messina and J. M. Ruso, Structural and Kinetic Visualization of the Protein Corona on Bioceramic Nanoparticles, *Langmuir*, 2018, **34**(7), 2471–2480.

33 S. Lara, F. Alnasser, E. Polo, D. Garry, M. C. Lo Giudice, D. R. Hristov, L. Rocks, A. Salvati, Y. Yan and K. A. Dawson, Identification of receptor binding to the biomolecular corona of nanoparticles, *ACS Nano*, 2017, **11**(2), 1884–1893.

34 H. Tanoue, N. L. Yamada, K. Ito and H. Yokoyama, Quantitative Analysis of Polymer Brush Formation Kinetics Using Quartz Crystal Microbalance: Viscoelasticity of Polymer Brush, *Langmuir*, 2017, **33**(21), 5166–5172.

35 L. Chai and J. Klein, Shear behavior of adsorbed poly (ethylene oxide) layers in aqueous media, *Macromolecules*, 2008, **41**(5), 1831–1838.

36 U. Raviv, J. Frey, R. Sak, P. Laurat, R. Tadmor and J. Klein, Properties and interactions of physigrafted end-functionalized poly (ethylene glycol) layers, *Langmuir*, 2002, **18**(20), 7482–7495.

37 M. Heuberger, T. Drobek and N. D. Spencer, Interaction forces and morphology of a protein-resistant poly (ethylene glycol) layer, *Biophys. J.*, 2005, **88**(1), 495–504.

38 S. Sharma, R. W. Johnson and T. A. Desai, XPS and AFM analysis of antifouling PEG interfaces for microfabricated silicon biosensors, *Biosens. Bioelectron.*, 2004, **20**(2), 227–239.

39 Y. Luan, D. Li, T. Wei, M. Wang, Z. Tang, J. L. Brash and H. Chen, "Hearing loss" in qcm measurement of protein adsorption to protein resistant polymer brush layers, *Anal. Chem.*, 2017, **89**(7), 4184–4191.

40 T. Drobek and N. D. Spencer, Nanotribology of surface-grafted PEG layers in an aqueous environment, *Langmuir*, 2008, **24**(4), 1484–1488.

41 D. R. Hristov, D. Ye, J. M. de Araújo, C. Ashcroft, B. DiPaolo, R. Hart, C. Earhart, H. Lopez and K. A. Dawson, Using single nanoparticle tracking obtained by nanophotonic force microscopy to simultaneously characterize nanoparticle size distribution and nanoparticle–surface interactions, *Nanoscale*, 2017, **9**(13), 4524–4535.

42 M. Wu, A. M. Vartanian, G. Chong, A. K. Pandiakumar, R. J. Hamers, R. Hernandez and C. J. Murphy, Solution NMR Analysis of Ligand Environment in Quaternary Ammonium-Terminated Self-Assembled Monolayers on Gold Nanoparticles: The Effect of Surface Curvature and Ligand Structure, *J. Am. Chem. Soc.*, 2019, **141**(10), 4316–4327.

43 J. Schaefer, C. Schulze, E. E. J. Marxer, U. F. Schaefer, W. Wohlleben, U. Bakowsky and C.-M. Lehr, Atomic force microscopy and analytical ultracentrifugation for probing nanomaterial protein interactions, *ACS Nano*, 2012, **6**(6), 4603–4614.

44 L. Polito, M. Colombo, D. Monti, S. Melato, E. Caneva and D. Prosperi, Resolving the structure of ligands bound to the surface of superparamagnetic iron oxide nanoparticles by high-resolution magic-angle spinning NMR spectroscopy, *J. Am. Chem. Soc.*, 2008, **130**(38), 12712–12724.

45 C. Charlier, S. N. Khan, T. Marquardsen, P. Pelupessy, V. Reiss, D. Sakellariou, G. Bodenhausen, F. Engelke and F. Ferrage, Nanosecond time scale motions in proteins revealed by high-resolution NMR relaxometry, *J. Am. Chem. Soc.*, 2013, **135**(49), 18665–18672.

46 R. Augustyniak, F. Ferrage, R. Paquin, O. Lequin and G. Bodenhausen, Methods to determine slow diffusion coefficients of biomolecules. Applications to Engrailed 2, a partially disordered protein, *J. Biomol. NMR*, 2011, **50**(3), 209–218.

47 Z. Varga, A. Wacha, U. Vainio, J. Gummel and A. Bóta, Characterization of the PEG layer of sterically stabilized liposomes: a SAXS study, *Chem. Phys. Lipids*, 2012, **165**(4), 387–392.

48 O. Kohlmann, W. E. Steinmetz, X.-A. Mao, W. P. Wuelfing, A. C. Templeton, R. W. Murray and C. S. Johnson, NMR diffusion, relaxation, and spectroscopic studies of water soluble, monolayer-protected gold nanoclusters, *J. Phys. Chem. B*, 2001, **105**(37), 8801–8809.

49 X. Liu, M. Yu, H. Kim, M. Mameli and F. Stellacci, Determination of monolayer-protected gold nanoparticle ligand–shell morphology using NMR, *Nat. Commun.*, 2012, **3**, 1182.

50 K. Salorinne, S. Malola, O. A. Wong, C. D. Rithner, X. Chen, C. J. Ackerson and H. Häkkinen, Conformation and dynamics of the ligand shell of a water-soluble Au102 nanoparticle, *Nat. Commun.*, 2016, **7**, 10401.

51 Y. Zhang, C. G. Fry, J. A. Pedersen and R. J. Hamers, Dynamics and morphology of nanoparticle-linked polymers elucidated by nuclear magnetic resonance, *Anal. Chem.*, 2017, **89**(22), 12399–12407.

 This journal is © The Royal Society of Chemistry 2021

Published on 22 February 2021. Downloaded by TU Dublin on 4/4/2022 10:07:53 AM.

52 H. Zhou, F. Du, X. Li, B. Zhang, W. Li and B. Yan, Characterization of organic molecules attached to gold nanoparticle surface using high resolution magic angle spinning ^{1}H NMR, *J. Phys. Chem. C*, 2008, **112**(49), 19360–19366.
53 C. L. Henoumont, S. Laurent, R. N. Muller and L. Vander Elst, HR-MAS NMR spectroscopy: An innovative tool for the characterization of iron oxide nanoparticles tracers for molecular imaging, *Anal. Chem.*, 2015, **87**(3), 1701–1710.
54 R. Sharma, G. P. Holland, V. C. Solomon, H. Zimmermann, S. Schiffenhaus, S. A. Amin, D. A. Buttry and J. L. Yarger, NMR characterization of ligand binding and exchange dynamics in triphenylphosphine-capped gold nanoparticles, *J. Phys. Chem. C*, 2009, **113**(37), 16387–16393.
55 R. H. Terrill, T. A. Postlethwaite, C.-h. Chen, C.-D. Poon, A. Terzis, A. Chen, J. E. Hutchison, M. R. Clark and G. Wignall, Monolayers in three dimensions: NMR, SAXS, thermal, and electron hopping studies of alkanethiol stabilized gold clusters, *J. Am. Chem. Soc.*, 1995, **117**(50), 12537–12548.
56 S. Fullam, H. Rensmo, S. N. Rao and D. Fitzmaurice, Noncovalent self-assembly of silver and gold nanocrystal aggregates in solution, *Chem. Mater.*, 2002, **14**(9), 3643–3650.
57 M. Garcia-Fuentes, D. Torres, M. Martín-Pastor and M. J. Alonso, Application of NMR spectroscopy to the characterization of PEG-stabilized lipid nanoparticles, *Langmuir*, 2004, **20**(20), 8839–8845.
58 E. M. Clop, A. K. Chattah and M. A. Perillo, Water and membrane dynamics in suspensions of lipid vesicles functionalized with poly (ethylene glycol) s, *J. Phys. Chem. B*, 2014, **118**(23), 6150–6158.
59 E. Mahon, D. R. Hristov and K. A. Dawson, Stabilising fluorescent silica nanoparticles against dissolution effects for biological studies, *Chem. Commun.*, 2012, **48**(64), 7970–7972.
60 S. T. Milner, Polymer Brushes, *Science*, 1991, **251**(4996), 905–914.
61 S. T. Milner, T. A. Witten and M. E. Cates, Theory of the grafted polymer brush, *Macromolecules*, 1988, **21**(8), 2610–2619.
62 H. I. Labouta, M. J. Gomez-Garcia, C. D. Sarsons, T. Nguyen, J. Kennard, W. Ngo, K. Terefe, N. Iragorri, P. Lai and K. D. Rinker, Surface-grafted polyethylene glycol conformation impacts the transport of PEG-functionalized liposomes through a tumour extracellular matrix model, *RSC Adv.*, 2018, **8**(14), 7697–7708.
63 P. De Gennes, Polymers at an interface; a simplified view, *Adv. Colloid Interface Sci.*, 1987, **27**(3–4), 189–209.
64 M. Cui, R. Liu, Z. Deng, G. Ge, Y. Liu and L. Xie, Quantitative study of protein coronas on gold nanoparticles with different surface modifications, *Nano Res.*, 2014, **7**(3), 345–352.
65 F. Simonelli, G. Rossi and L. Monticelli, Role of Ligand Conformation on Nanoparticle–Protein Interactions, *J. Phys. Chem. B*, 2019, **123**(8), 1764–1769.
66 C. Allen, N. Dos Santos, R. Gallagher, G. Chiu, Y. Shu, W. Li, S. Johnstone, A. Janoff, L. Mayer and M. Webb, Controlling the physical behavior and biological performance of liposome formulations through use of surface grafted poly (ethylene glycol), *Biosci. Rep.*, 2002, **22**(2), 225–250.
67 L. D. Unsworth, H. Sheardown and J. L. Brash, Protein resistance of surfaces prepared by sorption of end-thiolated poly (ethylene glycol) to gold: effect of surface chain density, *Langmuir*, 2005, **21**(3), 1036–1041.